
Predictive Preference Learning from Human Interventions

Haoyuan Cai, Zhenghao Peng, Bolei Zhou

Department of Computer Science,
University of California, Los Angeles

Abstract

Learning from human involvement aims to incorporate the human subject to monitor and correct agent behavior errors. Although most interactive imitation learning methods focus on correcting the agent’s action at the current state, they do not adjust its actions in future states, which may be potentially more hazardous. To address this, we introduce Predictive Preference Learning from Human Interventions (PPL), which leverages the implicit preference signals contained in human interventions to inform predictions of future rollouts. The key idea of PPL is to bootstrap each human intervention into L future time steps, called the preference horizon, with the assumption that the agent follows the same action and the human makes the same intervention in the preference horizon. By applying preference optimization on these future states, expert corrections are propagated into the safety-critical regions where the agent is expected to explore, significantly improving learning efficiency and reducing human demonstrations needed. We evaluate our approach with experiments on both autonomous driving and robotic manipulation benchmarks and demonstrate its efficiency and generality. Our theoretical analysis further shows that selecting an appropriate preference horizon L balances coverage of risky states with label correctness, thereby bounding the algorithmic optimality gap. Demo and code are available at: <https://metadriverse.github.io/ppl>.

1 Introduction

Effectively leveraging human demonstrations to teach and align autonomous agents remains a central challenge in both Reinforcement Learning (RL) [46] and Imitation Learning (IL) [17]. In the literature of RL and more recent RL from Human Feedback (RLHF), the agent explores the environment through trial and error or under human feedback guidance, and the learning process hinges on a carefully crafted reward function that reflects human preferences. However, RL algorithms often require a large number of environment interactions to learn stable policies, and their exploration can lead agents to dangerous or task-irrelevant states [40, 27]. In contrast, IL methods train agents to emulate human behavior using offline demonstrations from experts. Nevertheless, IL agents are susceptible to distributional shift because the offline dataset may lack corrective samples in safety-critical or out-of-distribution states [35, 32, 3, 47].

Interactive Imitation Learning (IIL) [2, 34, 15, 42, 28, 41, 19, 20] incorporates human participants to intervene in the training process and provide online demonstrations. Such methods have improved alignment and learning efficiency in a wide variety of tasks, including robot manipulation [7, 8], autonomous driving [27, 28], and even the strategy game StarCraft II [39]. One line of research on confidence-based IIL designs various task-specific criteria to request human help, including uncertainty estimation [23] and confidence in completing the task [4, 38]. In contrast, an increasing body of work focuses on learning from active human involvement, where human subjects actively intervene and provide demonstrations during training when the agent makes mistakes [15, 42, 22, 17, 28]. Compared to confidence-based IIL, active human involvement can ensure training safety [27].

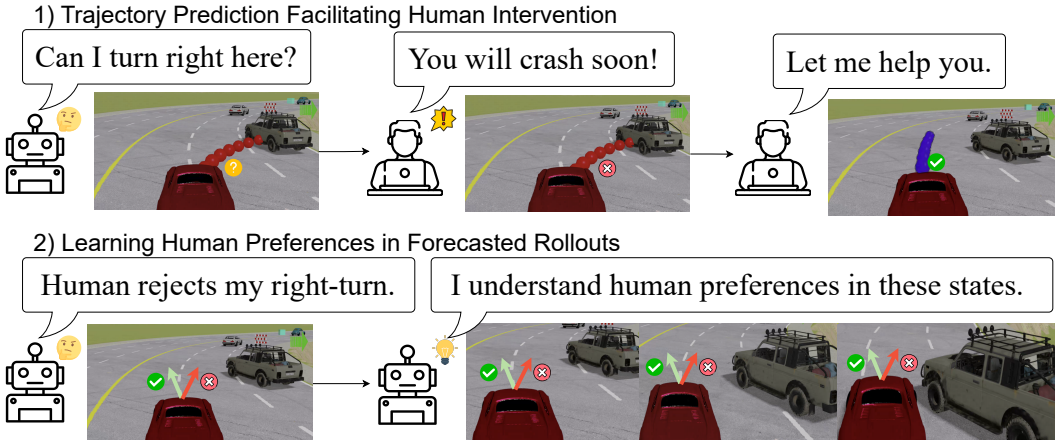


Figure 1: Our Predictive Preference Learning from Human Interventions. (Top) Our approach forecasts the agent’s upcoming trajectory (the red dotted path) and visualizes it for the human expert, who will intervene if the forecasted path indicates an upcoming failure. (Bottom) A single intervention is then interpreted as hypothesized preference signals across the predicted states. These signals reflect the agent’s imputed imagination of what the expert would prefer, guiding the policy to avoid the risky maneuver in similar future contexts. This integration of proactive forecasting and preference learning accelerates policy improvement and reduces the total number of expert interventions required.

and does not require carefully designing human intervention criteria for each task [12]. However, these methods require the human expert to monitor the entire training process, predict the agent’s future trajectories, and intervene immediately in safety-critical states [28], imposing a significant cognitive burden on the human participant. In addition, these methods often correct the agent’s behavior only at the current intervened state, penalizing undesired actions step by step. For instance, in HG-Dagger [15], the agent is optimized to mimic human actions solely at the states where interventions occur. In practice, it is intuitive that the agent may repeat similar mistakes in the consecutive future steps $t + 1, \dots, t + L$ following an error at step t . As a result, the expert must repeatedly provide corrective demonstrations in these regions, compromising training efficiency [17].

In this work, we propose a novel Interactive Imitation Learning algorithm, ***Predictive Preference Learning*** from Human Interventions (PPL), to learn from active human involvement. As shown in Fig. 1, our approach has two key designs: First, we employ an efficient rollout-based trajectory prediction model to forecast the agent’s future states. These predicted rollouts are visualized in real time for the user, helping human supervisors proactively determine when an intervention is necessary. Second, our algorithm leverages preference learning on the predicted future trajectories to further improve the sample efficiency and reduce the expert demonstrations needed. Such designs bring three strengths: (1) They mitigate the distributional shift problem in IIL and improve training efficiency. By incorporating anticipated future states into the training process, our method constructs a richer dataset, especially in safety-critical situations. This expanded dataset offers more information than expert corrective demonstrations in human-intervened states only. (2) The preference learning reduces the agent’s visits to dangerous states, thus suppressing human interventions in safety-critical situations. (3) By visualizing the agent’s predicted future trajectories in the user interface, we significantly reduce the cognitive burden on the human supervisor to constantly anticipate the agent’s behavior.

Our contributions can be summarized as follows:

1. We introduce a novel Interactive Imitation Learning (IIL) algorithm that leverages trajectory prediction to inform human intervention and employs preference learning to deter the agent from returning to dangerous states.
2. We evaluate our algorithm on the MetaDrive [16] and Robosuite [49] benchmarks, using both neural experts and real human participants, showing that PPL requires fewer expert monitoring efforts and demonstrations to achieve near-optimal policies.
3. We present a theoretical analysis that derives an upper bound on the performance gap of our approach. This bound highlights that the efficacy of our method lies in reducing distributional shifts while preserving the quality of preference data.

2 Related Work

Learning from Human Involvement. Many works incorporate human involvement in the training loop to provide corrective actions in dangerous or repetitive states. For example, Human-Gated DAgger (HG-DAgger) [15], Ensemble-DAgger [23], Thrifty-DAgger [12], Sirius [19], and Intervention Weighted Regression (IWR) [22] perform imitation learning on human intervention data. These methods do not leverage data collected by agents or suppress undesired actions likely to be intervened by humans, leading to the agent’s susceptibility to entering hazardous states and thus harming sample efficiency. EGPO [27], PVP [28], and AIM [2] design proxy cost or value functions to suppress the frequency of human involvement. However, these approaches still require human supervisors to continuously monitor the agent’s behavior throughout training and anticipate potential failures that may necessitate intervention. This continuous oversight imposes a significant cognitive load on the human expert and can limit scalability. Furthermore, these methods do not exploit the agent’s predicted future trajectories that the expert might identify as potentially leading to undesirable outcomes, which necessitates repeated corrective demonstrations in such situations.

Preference-Based RL. A large body of work focuses on learning human preferences by ranking pairs of trajectories generated by the agent [6, 9, 34, 44, 37, 26]. One prominent paradigm, reinforcement learning from human feedback (RLHF), first trains a reward model on offline human preference data and then uses that model to guide policy optimization [6, 25, 43]. RLHF has achieved impressive results in domains ranging from Atari games [6] to large language models [25]. Alternatively, methods such as Direct Preference Optimization (DPO) [31], Contrastive Preference Optimization (CPO) [45], and related variants [1, 24] bypass explicit reward-model training and instead directly optimize the policy to satisfy preference labels via a classification loss.

However, applying RLHF and DPO to real-time control problems faces challenges due to the need for extensive human labeling of preference data [31]. These labels are inherently subjective and prone to noise [37]. Moreover, acquiring a high-quality preference dataset and achieving near-optimal policies often requires a substantial number of environment samples, thereby imposing a considerable burden on human experts [10]. In contrast, our framework elicits preferences in an online, interactive manner: experts review the agent’s predicted future trajectory at each decision point and intervene when a failure is anticipated; these interventions are then converted into contrastive preference labels. This real-time preference collection enables the policy to adapt continuously to the evolving state distribution and to receive targeted feedback precisely where it is most needed. In summary, our approach PPL bridges preference-based RL and imitation learning by demonstrating that DPO-style alignment techniques can be effectively adapted to control problems within an interactive imitation learning framework.

3 Problem Formulation

In this section, we introduce our settings of interactive imitation learning environments. We use the Markov decision process (MDP) $M = \langle \mathcal{S}, \mathcal{A}, \mathcal{P}, r, \gamma, d_0 \rangle$ to model the environment, which contains a state space \mathcal{S} , an action space \mathcal{A} , a state transition function $\mathcal{P} : \mathcal{S} \times \mathcal{A} \rightarrow \mathcal{S}$, a reward function $r : \mathcal{S} \times \mathcal{A} \rightarrow [R_{\min}, R_{\max}]$, a discount factor $\gamma \in (0, 1)$, and an initial state distribution $d_0 : \mathcal{S} \rightarrow [0, 1]$. We denote $\pi(a | s) : \mathcal{S} \times \mathcal{A} \rightarrow [0, 1]$ as a stochastic policy. Reinforcement learning (RL) aims to learn a *novice policy* $\pi_n(a|s)$ that maximizes the expected cumulative return

$$J(\pi_n) = \mathbb{E}_{\tau \sim P_{\pi_n}} [\sum_{t=0}^{\infty} \gamma^t r(s_t, a_t)], \text{ wherein } \tau = (s_0, a_0, s_1, a_1, \dots) \text{ is the trajectory sampled from trajectory distribution } P_{\pi_n} \text{ induced by } \pi_n, d_0 \text{ and } \mathcal{P}. \text{ We also define the discounted state distribution under policy } \pi_n \text{ as } d_{\pi_n}(s) = (1-\gamma) \mathbb{E}_{\tau \sim P_{\pi_n}} [\sum_{t=0}^{\infty} \gamma^t \mathbb{I}[s_t = s]]. \text{ In this work, we consider the reward-free setting where the agent has no access to the task reward function } r(s, a).$$

In imitation learning (IL), we assume that the human expert behavior a_h follows a *human policy* $\pi_h(a | s)$. The agent aims to learn π_n from human expert trajectories $\tau_h \sim P_{\pi_h}$, and it needs to optimize π_n to close the gap between $\tau_n \sim P_{\pi_n}$ and τ_h . Prior works on imitation learning have shown that using an offline expert demonstration dataset may lead to poor performance due to out-of-distribution states [36, 34, 41]. Therefore, interactive imitation learning (IIL) methods incorporate a human expert into the training loop to provide online corrective demonstrations, making

the state distribution of expert data more similar to that of the novice policy [28, 35]. During training, the human expert monitors the agent and can intervene and take control if the agent’s action a_n at the current state s violates the human’s desired behavior or leads to a dangerous situation. We use the deterministic intervention policy $I(s, a_n) : \mathcal{S} \times \mathcal{A} \rightarrow \{0, 1\}$ to model the human’s intervention behavior, where the agent’s action follows the novice policy $a_n \sim \pi_n(\cdot | s)$, and the human subject takes control when $I(s, a_n) = 1$.

With the notations above, the agent’s actual trajectories during training are derived from the following shared *behavior policy*

$$\pi_b(a | s) = \pi_n(a | s)(1 - I(s, a)) + \pi_h(a | s)G(s), \quad (1)$$

wherein $G(s) = \int_{a' \in \mathcal{A}} I(s, a') \pi_n(a' | s) da'$ is the probability of the agent taking an action a_n that will be rejected and intervened by the human expert.

Preference Alignment. Recent works on preference-based RL have also leveraged offline preference datasets to learn human-aligned policies [31, 45, 1]. Given an offline preference dataset $\mathcal{D}_{\text{pref}}$ where each preference data $(s, a^+, a^-) \in \mathcal{D}_{\text{pref}}$ means that the human expert prefers the action a^+ over a^- at state s , we can learn an agent policy π_θ that aligns with the human preference model. The Contrastive Preference Optimization method [45] uses the following objective to train an agent policy π_θ from the preference dataset $\mathcal{D}_{\text{pref}}$:

$$\mathcal{L}_{\text{pref}}(\pi_\theta) = - \mathbb{E}_{(s, a^+, a^-) \sim \mathcal{D}_{\text{pref}}} [\log \sigma(\beta \log \pi_\theta(a^+ | s) - \beta \log \pi_\theta(a^- | s))], \quad (2)$$

where $\sigma(\cdot)$ is the Sigmoid function, and $\beta > 0$ is a hyperparameter.

Trajectory Prediction Model. In this work, we allow the agent to access a short-term trajectory prediction model $f(s, a_n, H)$. Given the current state s and the agent’s action a_n , we can predict the agent’s trajectory $f(s, a_n, H) = (s, \tilde{s}_1, \dots, \tilde{s}_H)$ in the next H steps, where \tilde{s}_i the predicted state that the agent will reach if the agent applies the action a_n for i steps from the state s . The implementation detail of f is in Sec. 4.3.

4 Method

4.1 Predictive Preference Learning from Human Interventions (PPL)

We propose PPL (Fig. 2), an efficient interactive imitation learning method that emulates the human policy with fewer expert demonstrations and less cognitive effort. The key idea of PPL is to learn human preferences from data generated by a future-trajectory prediction model. We illustrate the human-agent interactions in Fig. 2 (left) and how PPL infers human preference in Fig. 2 (right).

During training, the human subject monitors the agent-environment interaction in each state s (Fig. 2 (left)). The novice policy π_n suggests an action a_n for the current state s . Instead of executing a_n immediately, we query the trajectory prediction model $f(s, a_n, H)$ to obtain a predicted rollout $\tau = f(s, a_n, H) = (s, \tilde{s}_1, \dots, \tilde{s}_H)$, which we visualize for the human expert. The expert then uses τ to determine whether the agent will fail in the next H steps, such as crashing into vehicles or going off the road. If so, the expert will provide corrective actions $a_h \sim \pi_h(s)$ for the next H steps, depicted by the blue trajectory in Fig. 2. If the expert believes no intervention is needed, the agent continues to use its own policy π_n for the next H steps.

We introduce preference learning on the predicted trajectories because it is difficult to learn corrective behavior purely from the expert’s demonstrations in safe states. By visualizing predicted rollouts, experts can anticipate unsafe trajectories before the agent actually enters them and intervene preemptively. As a result, the state distribution covered by these early interventions differs substantially from the on-policy distribution of the novice policy, creating a distributional shift that standard imitation or on-policy correction cannot address. Therefore, instead of relying solely on expert demonstrations, we collect preference labels over the predicted rollouts (Fig. 2 Right) so that the agent can learn the correct behavior in those risky states.

Whenever the expert intervenes at state s , we interpret this as indicating that continuing with a_n would lead to unsafe or undesirable outcomes along the predicted trajectory. As shown in Fig. 2 (right), to capture this preference, we assume the expert prefers a_h over a_n at state s and each of

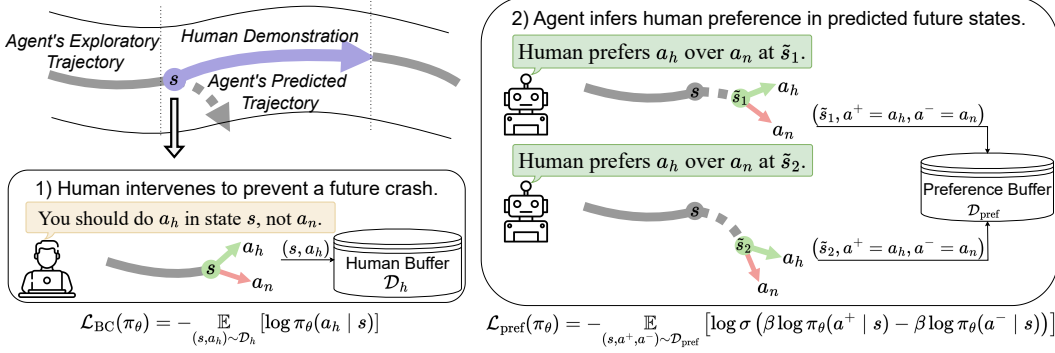


Figure 2: Illustration of Predictive Preference Learning. (Left) At each decision point, the agent proposes an action, and its future trajectory is predicted and visualized. The human expert reviews this rollout and intervenes only when a potential failure is anticipated. The intervention is recorded alongside the state into the human buffer \mathcal{D}_h for behavioral cloning. (Right) Each recorded intervention is then converted into contrastive preference pairs over the predicted future states $\tilde{s}_1, \dots, \tilde{s}_L$. These preference tuples are stored in a preference buffer \mathcal{D}_{pref} and used to train the policy via a contrastive classification loss, propagating expert intents into regions the agent is likely to explore.

the first L predicted states $\tilde{s}_1, \dots, \tilde{s}_L$ for some preference horizon $L \leq H$. For each $i \leq L$, we add the tuple $(\tilde{s}_i, a^+ = a_h, a^- = a_n)$ to the preference dataset \mathcal{D}_{pref} . We note that in each tuple $(\tilde{s}_i, a^+ = a_h, a^- = a_n)$, both a_h and a_n are sampled at the current state s , not the predicted future states \tilde{s}_i , because the exact human corrective actions at hypothetical future states are not directly observable. Still, the expert intervention at state s implies that applying a_h at the predicted states $\tilde{s}_1, \dots, \tilde{s}_L$, rather than continuing with a_n , is more likely to prevent the dangerous outcome in the end of the predicted trajectory (\tilde{s}_H). Hence, our construction of the preference dataset ensures that it faithfully captures the expert’s corrective intent across the predicted horizon.

The preference horizon L controls the length over which we elicit preferences in the predicted trajectory. A small L may fail to capture enough risky states, while a large L risks applying preferences where the corrective action a_h at state s no longer matches what an expert would do in those imagined states \tilde{s}_i . In Theorem 4.1, we prove that under mild assumptions, the performance gap of our learned policy is bounded by terms reflecting the state distribution shift and the quality of the preference labels, implying that an ideal preference horizon L should balance these two error terms. We also illustrate how the choice of L affects the performance of PPL in Fig. 8.

We train the novice policy π_n using two complementary objectives. First, we apply a behavioral cloning loss on expert demonstrations \mathcal{D}_h :

$$\mathcal{L}_{BC}(\pi_\theta) = - \mathbb{E}_{(s, a_h) \sim \mathcal{D}_h} [\log \pi_\theta(a_h | s)]. \quad (3)$$

Second, inspired by Contrastive Preference Optimization (CPO) [45], we use the preference-classification loss Eq. 2 over the predicted states in \mathcal{D}_{pref} . The final loss of the agent policy π_θ is evaluated as

$$\begin{aligned} \mathcal{L}(\pi_\theta) &= \mathcal{L}_{pref}(\pi_\theta) + \mathcal{L}_{BC}(\pi_\theta) \\ &= - \mathbb{E}_{(s, a^+, a^-) \sim \mathcal{D}_{pref}} [\log \sigma(\beta \log \pi_\theta(a^+ | s) - \beta \log \pi_\theta(a^- | s))] - \mathbb{E}_{(s, a_h) \sim \mathcal{D}_h} [\log \pi_\theta(a_h | s)]. \end{aligned} \quad (4)$$

The workflow of our method PPL is summarized in Alg. 1.

4.2 Analysis

We prove that the performance gap between the human policy π_h and the agent policy π_n can be bounded by the following three error terms: 1) the state distribution shift δ_{dist} , 2) the quality of the preference labels δ_{pref} , and 3) the optimization error ϵ .

The first error term is defined as $\delta_{dist} = D_{TV}(d_{\pi_n}, d_{\pi_h})$, where $d_{\pi_n}(s)$ is the discounted state distribution of the agent’s policy π_n , and $d_{\pi_h}(s) = |\mathcal{D}_{pref}|^{-1} \mathbb{E}_{(s', a^+, a^-) \sim \mathcal{D}_{pref}} \mathbb{I}[s' = s]$. Here,

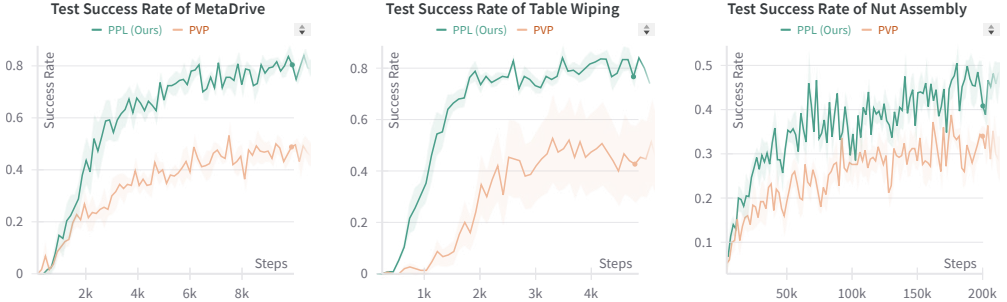


Figure 3: The test-time performance curve of PPL and the IIL counterpart PVP [28] under three different environments. The x-coordinate is the number of environment interactions, and the y-coordinate is the agent’s success rate in a held-out test environment, where the evaluation is conducted without expert involvement. Compared to the IIL counterpart, our approach achieves much higher learning efficiency and reduces the expert’s efforts needed.

$D_{\text{TV}}(P, Q) = \frac{1}{2}|P - Q|_1$ is the total variation distance between two distributions. This error term quantitatively measures the difference between the states actually visited by the agent and those contained in the preference dataset.

The second error term is defined as $\delta_{\text{pref}} = \mathbb{E}_{s \sim d_{\text{pref}}} D_{\text{TV}}(\rho_{\text{ideal}}^s, \rho_{\text{pref}}^s)$, which arises from the misalignment of the positive actions in the preference dataset, as the human action a_h in each tuple $(\tilde{s}_i, a_h, a_n) \in \mathcal{D}_{\text{pref}}$ is sampled in state s instead of state \tilde{s}_i . That is, this error reflects the assumption that the human would still apply the same corrective action a_h in a hypothetical future state \tilde{s}_i reached after executing a_n for i steps, which may not perfectly match what the expert would actually do. For any state s in $\mathcal{D}_{\text{pref}}$ with $d_{\text{pref}}(s) > 0$, the empirical preference-pair distribution in state s follows

$$\rho_{\text{pref}}^s(a_h, a_n) = \frac{\mathbb{E}_{(s', a^+, a^-) \sim \mathcal{D}_{\text{pref}}} \mathbb{I}[s' = s, a^+ = a_h, a^- = a_n]}{\mathbb{E}_{(s', a^+, a^-) \sim \mathcal{D}_{\text{pref}}} \mathbb{I}[s' = s]}. \quad (5)$$

The ideal preference-pair distribution at any state s in $\mathcal{D}_{\text{pref}}$ is simply the joint distribution of (a_h, a_n) : $\rho_{\text{ideal}}^s(a_h, a_n) = \pi_h(a_h | s) \pi_n(a_n | s)$ on $\mathcal{A} \times \mathcal{A}$.

Finally, we define the optimization error of the agent policy π_n as $\epsilon = \mathcal{L}_{\text{pref}}(\pi_n) - \mathcal{L}_{\text{pref}}(\pi_h)$. We recall that $\mathcal{L}_{\text{pref}}(\pi) = -\mathbb{E}_{(s, a^+, a^-) \sim \mathcal{D}_{\text{pref}}} [\log \sigma(\beta \log \pi(a^+ | s) - \beta \log \pi(a^- | s))]$, where β is a positive constant and $\sigma(\cdot)$ is the Sigmoid function. Under these notations, we have the following Thm. 4.1.

Theorem 4.1. *We denote the Q-function of the human policy π_h as $Q^*(s, a)$. We assume that for any (s, a, a') , $|Q^*(s, a) - Q^*(s, a')| \leq U$, $|\log \pi_h(a | s) - \log \pi_h(a' | s)| \leq M$, and $|\log \pi_n(a | s) - \log \pi_n(a' | s)| \leq M$, where $U, M > 0$ are constants. When β is small enough, we have*

$$J(\pi_h) - J(\pi_n) = O(\sqrt{\epsilon + \delta_{\text{pref}}} + \delta_{\text{dist}}). \quad (6)$$

Here we explain the insights of Thm. 4.1 as follows. In our choice of the preference horizon L , the key is to balance the two error terms δ_{dist} and δ_{pref} . Recall that the distribution shift term δ_{dist} measures how close the state distributions are when there is no human intervention (d_{π_n}) and the state distribution represented in the preference dataset (d_{pref}). Increasing L decreases δ_{dist} because the preference dataset will contain more predicted states \tilde{s}_i from the agent’s future trajectories. In contrast, the preference error term δ_{pref} captures the misalignment between the true but unobserved human action at a future state $t' > t$ and the bootstrapped corrective action a_h at step t , which we assume would also apply at t' . Therefore, the longer the preference horizon, the larger δ_{pref} , because the difference between the human actions a_h in state s and the predicted \tilde{s}_L grows as L increases. In Fig. 8, we visualize the effects of L on the performance of PPL. We prove Thm. 4.1 in Appendix F.

4.3 Implementation Details

Tasks. As shown in Fig. 4, we conduct experiments on control tasks and manipulation tasks with different observation and action spaces. For the control task, we consider the MetaDrive driving

experiments [16], where the agent must navigate towards the destination in heavy-traffic scenes without crashing into obstacles or other vehicles. The agent uses the sensory state vector $s \in \mathbb{R}^{259}$ as its observation and outputs a control signal $a = (a_0, a_1) \in [-1, 1]^2$ representing the steering angle and the acceleration, respectively. We evaluate the agent’s learned policy in a held-out test environment separate from the training environments.

For manipulation tasks, we consider the Table Wiping and Nut Assembly tasks from the Robosuite environment [49]. In the Table Wiping task, the robot arm must learn to wipe the whiteboard surface and clean all of the markings. The positions of these markings are randomized at the beginning of each episode. The states are $s \in \mathbb{R}^{34}$ and actions are $a \in \mathbb{R}^6$ (3 translations in the XYZ axes and 3 rotations around the XYZ axes). In the Nut Assembly task, the robot must grab a metal ring from a random initial pose and place it over a target cylinder at a fixed location. The states are $s \in \mathbb{R}^{51}$ and actions are $a \in \mathbb{R}^7$, where the additional dimension in the action space represents opening or closing the gripper. In both manipulation tasks, the simulated UR5e robot arm uses fixed-impedance operational-space control to achieve the commanded pose.

Trajectory Prediction Model. In PPL, we need to predict the future states $f(s, a_n, H) = (s, \tilde{s}_{t+1}, \dots, \tilde{s}_{t+H})$ from the current state s . We implement f by running an H -step simulator rollout from the current state s , repeatedly applying action a_n to collect the sequence $(\tilde{s}_{t+1}, \dots, \tilde{s}_{t+H})$. This H -step simulator rollout runs at up to 1,000 fps on a CPU.

In real-world tasks such as autonomous driving, simulator rollouts often deviate from reality because vehicle dynamics parameters are imperfect and other traffic participants behave unpredictably. To predict future motion with minimal overhead, prior work directly propagates the ego-vehicle’s state through a physics model [18, 29, 13]. Following this approach, we use the kinematic bicycle model [30] to simulate $H = 10$ steps, assuming all other traffic participants remain stationary. Compared with the data-driven approaches [50, 5, 21], this rule-based predictor requires only forward integration of a single vehicle and produces short-term trajectories whose accuracy closely matches simulator rollouts. This lightweight extrapolation method runs at about 3,000 fps on a CPU, enabling real-time prediction with minimal overhead. Our ablation studies confirm that replacing the simulator with our bicycle-model predictions incurs negligible performance loss (Table 2, rows 9-10).

5 Experiments

5.1 Experimental Setting

Neural Policies as Proxy Human Policies. Experiments with real human participants are time-consuming and exhibit high variability between trials. Following the prior works on interactive imitation learning [10, 27], in addition to real-human experiments, we also incorporate neural policies in the training loop of PPL to approximate human policies in Table 3, 4, and 5. The neural experts are trained using PPO-Lagrangian [33] for 20 million environment steps.

In MetaDrive, the neural expert uses the following takeover rule when training all baselines and our method PPL: if the predicted trajectory $\tau = f(s, a_n, H)$ contains any safety violation, such as crashes or going off the road, or the average speed is too slow, the expert takes control for the next H steps. In RoboSuite, the neural expert intervenes when the cumulative reward over the predicted trajectory τ falls below a threshold ϵ . We set $\epsilon = 1$ for the Table Wiping task and $\epsilon = 2$ for the Nut Assembly task.

In Table 1, we report experiments involving real humans in the MetaDrive safety benchmark. In Table 3, Table 4, and Table 5, we report experiments with the neural policy as the proxy human policy in the MetaDrive, Table Wiping, and Nut Assembly tasks, respectively.

Evaluation Metrics. In the Table Wiping task and Nut Assembly task, we report the *success rate*, the ratio of episodes where the agent reaches the destination. In the MetaDrive safety benchmark, we also report the *episodic return* and *route completion rate* during evaluation. The route completion rate is the ratio of the agent’s successfully traveled distance to the length of the complete route.

We train each interactive imitation learning baseline five times using distinct random seeds. Then, we roll out 50 trajectories generated by each model in the held-out evaluation environment and average each evaluation metric as the model’s performance. During the evaluation, no expert is involved. The standard deviation is provided. We fix $H = 10$ for all the interactive imitation learning baselines. In

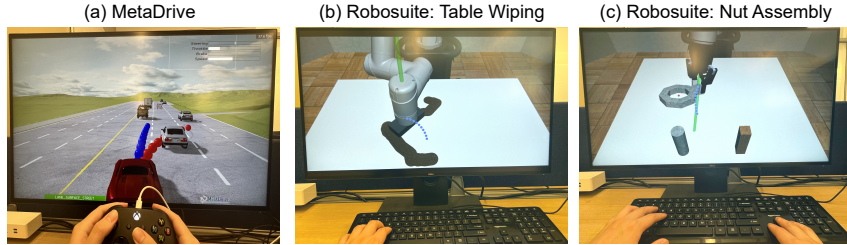


Figure 4: Human interfaces of the three tasks: MetaDrive (a), Table Wiping (b), and Nut Assembly (c). In (a), the agent’s forecasted trajectory (the red dots) leads to a collision, prompting the expert to intervene via the gamepad (blue dots show the predicted rollout of the expert). In (b) and (c), the expert observes the agent’s forecasted trajectory and intervenes via the keyboard if necessary.

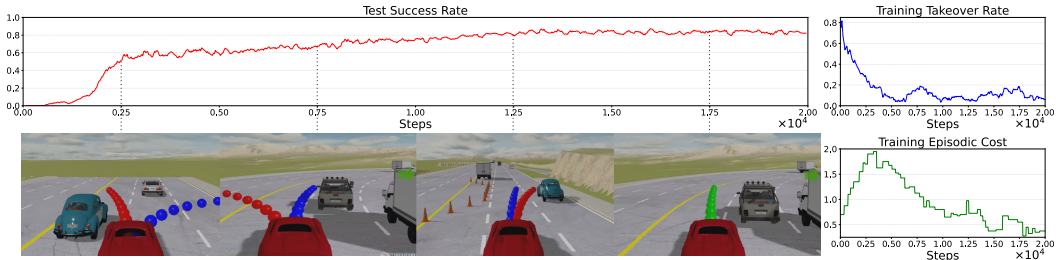


Figure 5: Training process of PPL in the MetaDrive environment with the human expert over 20K steps. We plot the test success rate (left), training takeover rate (top right), and training episodic safety cost (bottom right). During training, when the agent’s forecasted trajectory (red dots) leads to a collision, the human expert intervenes via the gamepad, and the corrected rollout is shown (blue dots). When the agent’s forecasted trajectory is safe, it is visualized in green dots. The agent becomes autonomous and performant during training, requiring fewer human interventions to maintain safety.

PPL, we fix $\beta = 0.1$, choose $L = 4$ for the MetaDrive benchmark and Table Wiping task, and set $L = 6$ for the Nut Assembly task. In Fig. 8, we show how the choice of L affects the performance of PPL in the MetaDrive benchmark.

We also report the total number of human-involved transitions (*human data usage*) and the *overall intervention rate*, which is the ratio of human data usage to total data usage. These show how much effort humans make to teach the agents.

Human Interfaces. Human subjects can take control through the Xbox Wireless Controller or the keyboard and monitor the training process by visualizing environments on the screen. The predicted trajectories are updated every $H = 10$ steps (one second), so that the human expert can intervene promptly before the agent causes any safety violations and undesired behaviors.

Baselines. We test two imitation learning baselines: Behavior Cloning (BC) and GAIL [11], and two confidence-based IIL methods: Ensemble-DAgger [23] and Thrifty-DAgger [12]. Four human-in-the-loop IIL methods that learn from active human involvement are tested: Intervention Weighted Regression (IWR) [22], Human-AI Copilot Optimization (HACO) [17], Expert Intervention Learning (EIL) [42], and Proxy Value Propagation [28].

5.2 Baseline Comparison

In Table 1, we report the performance of our PPL and all the baselines with real human experts in the MetaDrive safety benchmark. Our method PPL outperforms all the baselines and achieves a success rate of 76% within 10K steps. The whole experiment of PPL takes only 12 minutes on a desktop computer with an Nvidia GeForce RTX 4080 GPU.

In Table 3, 4, and 5, we report the performance of our PPL and all the baselines with neural experts as proxy human policies in MetaDrive, Table Wiping, and Nut Assembly tasks, respectively. We also plot the curves of the test-time success rate in Fig. 3. These tables and Fig. 3 show that PPL achieves both fewer expert data usage and environment samples needed in both driving tasks and

Table 1: Comparison of methods with training/testing statistics in the MetaDrive environment with the real human expert. The overall intervention rate is given together with the human data usage.

Method	Human-in-the-Loop	Training		Testing		
		Human Data Usage	Total Data Usage	Success Rate	Episodic Return	Route Completion
Human Expert	—	20K	—	0.95 ± 0.04	349.2 ± 18.2	0.98 ± 0.01
BC	✗	20K	—	0.0 ± 0.0	53.5 ± 22.8	0.16 ± 0.07
GAIL	✗	20K	1M	0.14 ± 0.03	146.2 ± 17.1	0.44 ± 0.05
Ensemble-DAgger	✓	3.8K (0.38)	10K	0.36 ± 0.11	233.8 ± 21.3	0.70 ± 0.02
Thrifty-DAgger	✓	3.2K (0.32)	10K	0.45 ± 0.04	221.5 ± 26.4	0.62 ± 0.04
PVP	✓	4.9K (0.49)	10K	0.46 ± 0.08	267.3 ± 15.0	0.71 ± 0.04
IWR	✓	5.2K (0.52)	10K	0.23 ± 0.10	246.7 ± 10.7	0.62 ± 0.02
EIL	✓	6.9K (0.69)	10K	0.01 ± 0.01	137.3 ± 26.1	0.40 ± 0.08
HACO	✓	6.3K (0.63)	10K	0.11 ± 0.05	154.7 ± 14.7	0.45 ± 0.09
PPL (Ours)	✓	2.9K (0.29)	10K	0.76 ± 0.07	324.8 ± 9.2	0.90 ± 0.06

Table 2: Ablation studies in MetaDrive with 10K total data usage. We use the neural expert as the proxy human policy.

Method	Expert Data Usage	Route Completion	Success Rate
Imitation on a^+	1.9K	0.65	0.36
PPL with random a^+	2.2K	0.73	0.45
PPL with random a^-	2.3K	0.69	0.38
PPL with DPO	1.6K	0.91	0.80
PPL with IPO	2.6K	0.61	0.35
PPL with SLiC-HF	3.0K	0.59	0.32
PPL with BC loss only	2.0K	0.72	0.42
PPL with CPO loss only	5.8K	0.31	0.04
PPL with rule-based f	1.9K	0.91	0.78
PPL (Ours)	1.8K	0.92	0.81

robot manipulation tasks while significantly outperforming baselines in testing performance. These results suggest that our construction of the preference dataset accurately reflects human preferences and helps speed up imitation learning. In addition, Fig. 6 shows that our method PPL produces smoother control sequences and generates trajectories that better align with human preferences.

5.3 Ablation Studies

In Table 2, we perform ablation studies of our PPL in the MetaDrive safety benchmark with the neural expert as proxy human policies.

Discarding positive or negative actions: In the first three rows of Table 2, we show that the advantage of our method PPL arises from the constructed preference pairs (\tilde{s}, a^+, a^-) in the preference data $\mathcal{D}_{\text{pref}}$ (Fig. 2 (right)), instead of merely emulating the positive actions a^+ or simply avoiding taking the negative actions a^- in the preference buffer. As shown in Table 2, discarding the negative actions a^- and performing Behavior Cloning on the positive actions (Imitation on a^+) leads to poor performance, which is even worse than directly imitating the expert demonstrations in the human buffer \mathcal{D}_h (PPL with BC loss only). In addition, replacing the positive actions by random actions (PPL with random a^+) or the negative actions by random actions (PPL with random a^-) also fails to solve the MetaDrive benchmark.

Preference-based RL objectives: In our learning objective Eq. 4, we use the Contrastive Preference Optimization (CPO) loss [45] to learn from the preference dataset $\mathcal{D}_{\text{pref}}$. In Table 2 (rows 4–6), we also report the performance of using other preference-based RL objectives from Direct Preference Optimization (DPO) [31], IPO [1], and SLiC-HF [48]. For DPO and IPO, we use a reference policy trained by Behavior Cloning from 10K expert demonstrations. Table 2 shows that using IPO (PPL with IPO) and SLiC-HF (PPL with SLiC-HF) objectives degrade the performance of PPL. Using the DPO objective (PPL with DPO) does not hurt the performance of PPL. However, the DPO objective requires access to a pretrained reference policy, while our learning objective Eq. 4 does not.

Discarding the BC loss or preference loss: As shown in row 7 of Table 2, discarding the CPO loss $\mathcal{L}_{\text{pref}}$ in Eq. 4 (PPL with BC loss only) significantly damages the performance of PPL. Discarding

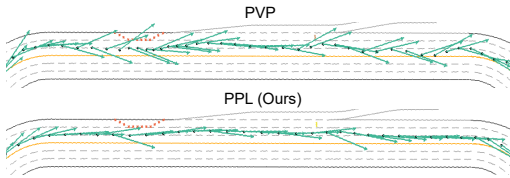


Figure 6: We plot the steering control sequences for both PVP and PPL on the same MetaDrive map, with arrows representing the steering angles every five steps. Both agents are trained to 10K steps. Compared to PVP, our method yields smoother steering and more consistent speeds, especially when navigating close to obstacles.

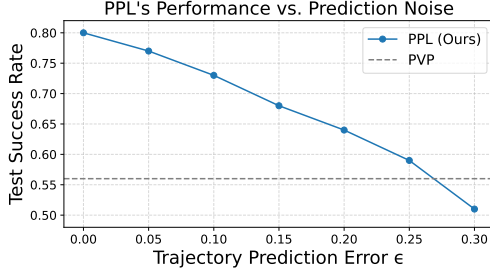


Figure 7: Performance of PPL under varying trajectory-prediction noise levels ϵ in MetaDrive. PPL still outperforms PVP when the trajectory predictor is imperfect.

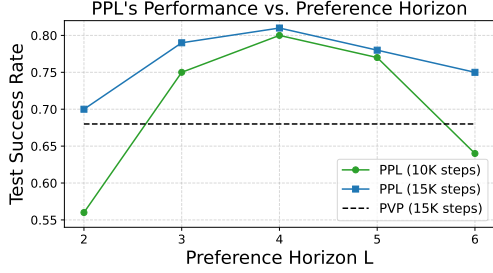


Figure 8: Performance of PPL with different preference horizons L in MetaDrive with 10K and 15K total data usage. PPL has the best learning efficiency when we set $L = 4$ in MetaDrive.

the BC loss (PPL with CPO loss only) also damages the performance, because the BC loss helps regularize our learned policy and avoid it deviating too much from the expert demonstrations.

Rule-based trajectory prediction model: Following Sec. 4.3, we also implement a rule-based trajectory prediction model f by simulating the ego-vehicle dynamics for H steps. Using a rule-based f (PPL with rule-based f) has negligible effects on the performance of PPL. This shows that our method still outperforms the IIL baselines even without relying on simulator rollouts.

5.4 Robustness Analysis

In Sec. 5.4, we evaluate PPL’s robustness to noise in the trajectory predictor (Fig. 7). We also visualize the effect of the preference horizon L on PPL in Fig. 8.

In Fig. 7, we show that PPL is robust to noise in trajectory predictors. With an imperfect predictive model, PPL still outperforms all the baselines. We inject random Gaussian noise e_{noise} to the outputs \tilde{s} of the trajectory predictor, and we set the norm $\|e_{\text{noise}}\|_2 = \epsilon * \|\tilde{s}\|_2$. Then we gradually increase the constant ϵ to test PPL’s robustness to noises in trajectory predictors. We use MetaDrive, Table Wiping, and Nut Assembly environments following the same setups from Tables 3, 4, and 5, respectively. We find that with a noisy predictive model, PPL still outperforms all the baselines in MetaDrive and Table Wiping when the noise $\epsilon \leq 0.25$. In Nut Assembly, PPL outperforms the baselines when $\epsilon \leq 0.125$.

In Fig. 8, we visualize how the preference horizon L affects the test success rate of PPL in the MetaDrive safety benchmark with 10K and 15K total data usage. As L increases from 2 to 4, the agent gains additional corrective information from forecasted states in the preference buffer and achieves higher success rates. Beyond $L = 4$, however, the benefit tapers off and eventually degrades, since overly long horizons yield less accurate preference labels. Therefore, we observe peak learning efficiency at $L = 4$. Notably, when $3 \leq L \leq 5$, PPL trained for only 10K steps already outperforms PVP trained for 15K steps. With an appropriately chosen preference horizon, PPL can substantially reduce both training time and expert monitoring effort.

6 Conclusion

In this work, we propose Predictive Preference Learning from Human Interventions (PPL), a novel interactive imitation learning algorithm that applies preference learning over predicted future trajectories to capture implicit human preferences. By converting each expert intervention into contrastive preference labels across forecasted states, PPL directs corrective feedback toward the regions of the state space the agent is most likely to explore. This approach substantially improves learning efficiency and reduces both the number of required demonstrations and the expert’s cognitive load, without offline pretraining and reward engineering.

Limitations. We assume that the expert always knows the optimal corrective action and demonstrates it accurately, whereas human demonstrations can be suboptimal or inconsistent. Additionally, all our experiments are conducted in simulation. The effectiveness and safety of PPL on real robots operating in physical environments remain to be explored in future works.

Acknowledgment: This work was supported by the NSF Grants CCF-2344955 and IIS-2339769, and ONR grant N000142512166. The human experiment in this study is approved through the IRB#23-000116 at UCLA. ZP was supported by the Amazon Fellowship via UCLA Science Hub.

References

- [1] Mohammad Gheshlaghi Azar, Zhaohan Daniel Guo, Bilal Piot, Remi Munos, Mark Rowland, Michal Valko, and Daniele Calandriello. A general theoretical paradigm to understand learning from human preferences. In *International Conference on Artificial Intelligence and Statistics*, pages 4447–4455. PMLR, 2024.
- [2] Haoyuan Cai, Zhenghao Peng, and Bolei Zhou. Robot-gated interactive imitation learning with adaptive intervention mechanism. *International Conference on Machine Learning*, 2025.
- [3] Sonia Chernova and Andrea L Thomaz. *Robot learning from human teachers*. Springer Nature, 2022.
- [4] Sonia Chernova and Manuela Veloso. Interactive policy learning through confidence-based autonomy. *Journal of Artificial Intelligence Research*, 34:1–25, 2009.
- [5] Cheng Chi, Zhenjia Xu, Siyuan Feng, Eric Cousineau, Yilun Du, Benjamin Burchfiel, Russ Tedrake, and Shuran Song. Diffusion policy: Visuomotor policy learning via action diffusion. *The International Journal of Robotics Research*, page 02783649241273668, 2023.
- [6] Paul F. Christiano, Jan Leike, Tom B. Brown, Miljan Martic, Shane Legg, and Dario Amodei. Deep reinforcement learning from human preferences. In Isabelle Guyon, Ulrike von Luxburg, Samy Bengio, Hanna M. Wallach, Rob Fergus, S. V. N. Vishwanathan, and Roman Garnett, editors, *Advances in Neural Information Processing Systems 30: Annual Conference on Neural Information Processing Systems 2017, December 4-9, 2017, Long Beach, CA, USA*, pages 4299–4307, 2017.
- [7] Bin Fang, Shidong Jia, Di Guo, Muhua Xu, Shuhuan Wen, and Fuchun Sun. Survey of imitation learning for robotic manipulation. *International Journal of Intelligent Robotics and Applications*, 3:362–369, 2019.
- [8] Aditya Ganapathi, Priya Sundaresan, Brijen Thananjeyan, Ashwin Balakrishna, Daniel Seita, Jennifer Grannen, Minho Hwang, Ryan Hoque, Joseph E Gonzalez, Nawid Jamali, et al. Learning dense visual correspondences in simulation to smooth and fold real fabrics. In *2021 IEEE International Conference on Robotics and Automation (ICRA)*, pages 11515–11522. IEEE, 2021.
- [9] Lin Guan, Mudit Verma, Sihang Guo, Ruohan Zhang, and Subbarao Kambhampati. Widening the pipeline in human-guided reinforcement learning with explanation and context-aware data augmentation. *Advances in Neural Information Processing Systems*, 34, 2021.
- [10] Joey Hejna, Rafael Rafailov, Harshit Sikchi, Chelsea Finn, Scott Niekum, W Bradley Knox, and Dorsa Sadigh. Contrastive preference learning: learning from human feedback without rl. *arXiv preprint arXiv:2310.13639*, 2023.
- [11] Jonathan Ho and Stefano Ermon. Generative adversarial imitation learning. In Daniel D. Lee, Masashi Sugiyama, Ulrike von Luxburg, Isabelle Guyon, and Roman Garnett, editors, *Advances in Neural Information Processing Systems 29: Annual Conference on Neural Information Processing Systems 2016, December 5-10, 2016, Barcelona, Spain*, pages 4565–4573, 2016.
- [12] Ryan Hoque, Ashwin Balakrishna, Ellen Novoseller, Albert Wilcox, Daniel S. Brown, and Ken Goldberg. Thriftydagger: Budget-aware novelty and risk gating for interactive imitation learning, 2021.
- [13] Nico Kaempchen, Bruno Schiele, and Klaus Dietmayer. Situation assessment of an autonomous emergency brake for arbitrary vehicle-to-vehicle collision scenarios. *IEEE Transactions on Intelligent Transportation Systems*, 10(4):678–687, 2009.
- [14] Sham M. Kakade and John Langford. Approximately optimal approximate reinforcement learning. In Claude Sammut and Achim G. Hoffmann, editors, *Machine Learning, Proceedings of the Nineteenth International Conference (ICML 2002), University of New South Wales, Sydney, Australia, July 8-12, 2002*, pages 267–274. Morgan Kaufmann, 2002.
- [15] Michael Kelly, Chelsea Sidrane, Katherine Driggs-Campbell, and Mykel J Kochenderfer. Hg-dagger: Interactive imitation learning with human experts. In *2019 International Conference on Robotics and Automation (ICRA)*, pages 8077–8083. IEEE, 2019.

- [16] Quanyi Li, Zhenghao Peng, Lan Feng, Qihang Zhang, Zhenghai Xue, and Bolei Zhou. Metadrive: Composing diverse driving scenarios for generalizable reinforcement learning. *IEEE transactions on pattern analysis and machine intelligence*, 2022.
- [17] Quanyi Li, Zhenghao Peng, and Bolei Zhou. Efficient learning of safe driving policy via human-ai copilot optimization. In *International Conference on Learning Representations*, 2022.
- [18] Chiu-Feng Lin, A Galip Ulsoy, and David J LeBlanc. Vehicle dynamics and external disturbance estimation for vehicle path prediction. *IEEE Transactions on Control Systems Technology*, 8(3):508–518, 2000.
- [19] Huihan Liu, Soroush Nasiriany, Lance Zhang, Zhiyao Bao, and Yuke Zhu. Robot learning on the job: Human-in-the-loop autonomy and learning during deployment. *The International Journal of Robotics Research*, page 02783649241273901, 2022.
- [20] Huihan Liu, Yu Zhang, Vaarij Betala, Evan Zhang, James Liu, Crystal Ding, and Yuke Zhu. Multi-task interactive robot fleet learning with visual world models. *arXiv preprint arXiv:2410.22689*, 2024.
- [21] Yicheng Liu, Jinghuai Zhang, Liangji Fang, Qinzhong Jiang, and Bolei Zhou. Multimodal motion prediction with stacked transformers. In *Proceedings of the IEEE/CVF conference on computer vision and pattern recognition*, pages 7577–7586, 2021.
- [22] Ajay Mandlekar, Danfei Xu, Roberto Martín-Martín, Yuke Zhu, Li Fei-Fei, and Silvio Savarese. Human-in-the-loop imitation learning using remote teleoperation. *ArXiv preprint*, abs/2012.06733, 2020.
- [23] Kunal Menda, Katherine Driggs-Campbell, and Mykel J Kochenderfer. Ensembledagger: A bayesian approach to safe imitation learning. In *2019 IEEE/RSJ International Conference on Intelligent Robots and Systems (IROS)*, pages 5041–5048. IEEE, 2019.
- [24] Yu Meng, Mengzhou Xia, and Danqi Chen. Simpo: Simple preference optimization with a reference-free reward. *Advances in Neural Information Processing Systems*, 37:124198–124235, 2024.
- [25] Long Ouyang, Jeff Wu, Xu Jiang, Diogo Almeida, Carroll L Wainwright, Pamela Mishkin, Chong Zhang, Sandhini Agarwal, Katarina Slama, Alex Ray, et al. Training language models to follow instructions with human feedback. *arXiv preprint arXiv:2203.02155*, 2022.
- [26] Malayandi Palan, Gleb Shevchuk, Nicholas Charles Landolfi, and Dorsa Sadigh. Learning reward functions by integrating human demonstrations and preferences. In *Robotics: Science and Systems*, 2019.
- [27] Zhenghao Peng, Quanyi Li, Chunxiao Liu, and Bolei Zhou. Safe driving via expert guided policy optimization. In *5th Annual Conference on Robot Learning*, 2021.
- [28] Zhenghao Mark Peng, Wenjie Mo, Chenda Duan, Quanyi Li, and Bolei Zhou. Learning from active human involvement through proxy value propagation. *Advances in neural information processing systems*, 36, 2024.
- [29] Romain Pepy, Alain Lambert, and Hugues Mounier. Reducing navigation errors by planning with realistic vehicle model. In *2006 IEEE Intelligent Vehicles Symposium*, pages 300–307. IEEE, 2006.
- [30] Philip Polack, Florent Altché, Brigitte d’Andréa Novel, and Arnaud de La Fortelle. The kinematic bicycle model: A consistent model for planning feasible trajectories for autonomous vehicles? In *2017 IEEE intelligent vehicles symposium (IV)*, pages 812–818. IEEE, 2017.
- [31] Rafael Rafailov, Archit Sharma, Eric Mitchell, Christopher D Manning, Stefano Ermon, and Chelsea Finn. Direct preference optimization: Your language model is secretly a reward model. *Advances in Neural Information Processing Systems*, 36:53728–53741, 2023.
- [32] Harish Ravichandar, Athanasios S Polydoros, Sonia Chernova, and Aude Billard. Recent advances in robot learning from demonstration. *Annual Review of Control, Robotics, and Autonomous Systems*, 3:297–330, 2020.
- [33] Alex Ray, Joshua Achiam, and Dario Amodei. Benchmarking safe exploration in deep reinforcement learning. *arXiv preprint arXiv:1910.01708*, 7(1):2, 2019.
- [34] Siddharth Reddy, Anca D Dragan, and Sergey Levine. Shared autonomy via deep reinforcement learning. *Robotics: Science and Systems*, 2018.
- [35] Stéphane Ross and Drew Bagnell. Efficient reductions for imitation learning. In *Proceedings of the thirteenth international conference on artificial intelligence and statistics*, pages 661–668. JMLR Workshop and Conference Proceedings, 2010.

- [36] Stéphane Ross, Geoffrey Gordon, and Drew Bagnell. A reduction of imitation learning and structured prediction to no-regret online learning. In *Proceedings of the fourteenth international conference on artificial intelligence and statistics*, pages 627–635. JMLR Workshop and Conference Proceedings, 2011.
- [37] Dorsa Sadigh, Anca D Dragan, Shankar Sastry, and Sanjit A Seshia. Active preference-based learning of reward functions. *UC Berkeley*, 2017.
- [38] H. Saeidi, Justin D. Opfermann, Michael Kam, Sudarshan Raghunathan, S. Leonard, and A. Krieger. A confidence-based shared control strategy for the smart tissue autonomous robot (star). In *2018 IEEE/RSJ International Conference on Intelligent Robots and Systems (IROS)*, pages 1268–1275, 2018.
- [39] Mikayel Samvelyan, Tabish Rashid, Christian Schroeder De Witt, Gregory Farquhar, Nantas Nardelli, Tim GJ Rudner, Chia-Man Hung, Philip HS Torr, Jakob Foerster, and Shimon Whiteson. The starcraft multi-agent challenge. *ArXiv preprint*, abs/1902.04043, 2019.
- [40] William Saunders, Girish Sastry, Andreas Stuhlmüller, and Owain Evans. Trial without error: Towards safe reinforcement learning via human intervention. In *Proceedings of the 17th International Conference on Autonomous Agents and MultiAgent Systems*, pages 2067–2069. International Foundation for Autonomous Agents and Multiagent Systems, 2018.
- [41] Esmaeil Seraj, Kin Man Lee, Zulfiqar Zaidi, Qingyu Xiao, Zhaoxin Li, Arthur Nascimento, Sanne van Waveren, Pradyumna Tambwekar, Rohan Paleja, Devleena Das, et al. Interactive and explainable robot learning: A comprehensive review. *Foundations and Trends® in Robotics*, 12(2-3):75–349, 2024.
- [42] Jonathan Spencer, Sanjiban Choudhury, Matthew Barnes, Matthew Schmittie, Mung Chiang, Peter Ramadge, and Siddhartha Srinivasa. Learning from interventions. In *Robotics: Science and Systems (RSS)*, 2020.
- [43] Nisan Stiennon, Long Ouyang, Jeffrey Wu, Daniel Ziegler, Ryan Lowe, Chelsea Voss, Alec Radford, Dario Amodei, and Paul F Christiano. Learning to summarize with human feedback. *Advances in neural information processing systems*, 33:3008–3021, 2020.
- [44] Garrett Warnell, Nicholas R. Waytowich, Vernon Lawhern, and Peter Stone. Deep TAMER: interactive agent shaping in high-dimensional state spaces. In Sheila A. McIlraith and Kilian Q. Weinberger, editors, *Proceedings of the Thirty-Second AAAI Conference on Artificial Intelligence, (AAAI-18), the 30th innovative Applications of Artificial Intelligence (IAAI-18), and the 8th AAAI Symposium on Educational Advances in Artificial Intelligence (EAAI-18), New Orleans, Louisiana, USA, February 2-7, 2018*, pages 1545–1554. AAAI Press, 2018.
- [45] Haoran Xu, Amr Sharaf, Yunmo Chen, Weiting Tan, Lingfeng Shen, Benjamin Van Durme, Kenton Murray, and Young Jin Kim. Contrastive preference optimization: Pushing the boundaries of llm performance in machine translation. *arXiv preprint arXiv:2401.08417*, 2024.
- [46] Zhenghai Xue, Zhenghao Peng, Quanyi Li, Zhihan Liu, and Bolei Zhou. Guarded policy optimization with imperfect online demonstrations. *arXiv preprint arXiv:2303.01728*, 2023.
- [47] Maryam Zare, Parham M Kebria, Abbas Khosravi, and Saeid Nahavandi. A survey of imitation learning: Algorithms, recent developments, and challenges. *IEEE Transactions on Cybernetics*, 2024.
- [48] Yao Zhao, Rishabh Joshi, Tianqi Liu, Misha Khalman, Mohammad Saleh, and Peter J Liu. Slic-hf: Sequence likelihood calibration with human feedback. *arXiv preprint arXiv:2305.10425*, 2023.
- [49] Yuke Zhu, Josiah Wong, Ajay Mandlekar, Roberto Martín-Martín, Abhishek Joshi, Soroush Nasiriany, and Yifeng Zhu. robosuite: A modular simulation framework and benchmark for robot learning. *arXiv preprint arXiv:2009.12293*, 2020.
- [50] Alex Zyner, Stewart Worrall, and Eduardo Nebot. A recurrent neural network solution for predicting driver intention at unsignalized intersections. *IEEE Robotics and Automation Letters*, 3(3):1759–1764, 2018.

A Algorithm

We summarize our method PPL in Alg. 1.

Algorithm 1 Predictive Preference Learning from Human Interventions (PPL)

```

1: Input: Hyperparameters  $H, L, \beta$ .
2: for timestep  $k = 0, H, 2H, \dots$  do
3:   Agent samples action  $a_n \sim \pi_n(s_k)$ .
4:   Predict future trajectory  $\tau = f(s_k, a_n, H) = (s_k, \tilde{s}_{k+1}, \dots, \tilde{s}_{k+H})$ .
5:   Human observes  $\tau$  to decide whether to take over in the next  $H$  steps.
6:   for timestep  $t = k, k + 1, \dots, k + H - 1$  do
7:     if Human takes over then
8:       Human takes action  $a_h \sim \pi_h(s_t)$ .
9:       Add  $(s_t, a_h)$  to the human buffer  $\mathcal{D}_h$ .
10:      Agent samples action  $a_n \sim \pi_n(s_t)$ .
11:      Predict future trajectory  $\tau' = f(s_t, a_n, L) = (s_t, \tilde{s}_{t+1}, \dots, \tilde{s}_{t+L})$ .
12:      Add  $(\tilde{s}, a_h, a_n)$  to the preference dataset  $\mathcal{D}_{\text{pref}}$  for each  $\tilde{s}$  in  $(s_t, \tilde{s}_{t+1}, \dots, \tilde{s}_{t+L})$ .
13:      Observe  $s_{t+1} \sim \mathcal{P}(\cdot | s_t, a_h)$ .
14:    else
15:      Agent samples action  $a_n \sim \pi_n(s_t)$ .
16:      Observe  $s_{t+1} \sim \mathcal{P}(\cdot | s_t, a_n)$ .
17:    end if
18:    Train policy  $\pi_n$  with loss function Eq. 4.
19:  end for
20: end for
21: Output: Policy  $\pi_n$ .

```

B Additional Experimental Results

We report the performance of our PPL and all the baselines with neural experts as proxy human policies in MetaDrive (Table 3), Table Wiping (Table 4), and Nut Assembly (Table 5) tasks, respectively. The test success rate curves of all three tasks are shown in Fig. 3.

Table 3: Comparison of methods with training/testing statistics in the MetaDrive environment with the neural expert as the proxy human policy. The overall intervention rate is given together with the expert data usage.

Method	Expert-in-the-Loop	Training		Testing		
		Expert Data Usage	Total Data Usage	Success Rate	Episodic Return	Route Completion
Neural Expert	—	—	—	0.83 ± 0.07	340.2 ± 15.9	0.93 ± 0.02
BC	✗	20K	—	0.12 ± 0.04	142.7 ± 27.5	0.46 ± 0.07
GAIL	✗	20K	1M	0.34 ± 0.08	196.5 ± 14.1	0.60 ± 0.09
Ensemble-DAgger	✓	3.2K (0.32)	10K	0.41 ± 0.08	238.6 ± 13.0	0.69 ± 0.07
Thrifty-DAgger	✓	2.9K (0.29)	10K	0.49 ± 0.07	248.2 ± 27.8	0.75 ± 0.06
PVP	✓	2.5K (0.25)	10K	0.56 ± 0.07	258.1 ± 23.4	0.76 ± 0.05
IWR	✓	2.7K (0.27)	10K	0.33 ± 0.11	217.0 ± 20.9	0.67 ± 0.06
EIL	✓	3.9K (0.39)	10K	0.11 ± 0.06	131.8 ± 29.5	0.42 ± 0.11
HACO	✓	2.6K (0.26)	10K	0.36 ± 0.15	210.2 ± 25.2	0.64 ± 0.10
PPL (Ours)	✓	1.2K (0.20)	6K	0.80 ± 0.04	329.9 ± 13.4	0.92 ± 0.03

Table 4: Results of different approaches in Table Wiping.

Method	Expert Data Usage	Total Data	Success Rate
Neural Expert	—	—	0.84
BC	10K	—	0.11
GAIL	10K	1M	0.37
PVP	2.3K	4K	0.58
IWR	2.5K	4K	0.51
EIL	2.4K	4K	0.53
HACO	2.9K	4K	0.48
PPL (Ours)	0.2K	2K	0.80

Table 5: Results of different approaches in Nut Assembly.

Method	Expert Data Usage	Total Data	Success Rate
Neural Expert	—	—	0.60
BC	100K	—	0.02
GAIL	100K	1M	0.08
PVP	49K	200K	0.35
IWR	54K	200K	0.29
EIL	48K	200K	0.25
HACO	77K	200K	0.15
PPL (Ours)	48K	200K	0.51

The neural experts in Table 3, 4, and 5 are trained with PPO-Lagrangian [33] for 20M environment steps, yet their test success rates still fall short of 100% for the following reasons. The MetaDrive safety environments occasionally generate rare but challenging scenarios that even a well-trained policy may fail to handle. In the Table Wiping task, the neural expert sometimes fails to remove one or two markings on the whiteboard, leaving a small patch of dirt uncleared. In the Nut Assembly task, successful grasping requires the gripper to be precisely aligned with the metal ring’s handle, which is highly sensitive to even minor action errors.

C Demo Video

We have attached our demo video to <https://metadrive.github.io/ppl>. This video shows how we conduct human experiments and the evaluation results of our method Predictive Preference Learning from Human Interventions (PPL). This video includes five sections:

1. The first section gives an overview of Predictive Preference Learning, showing what human observes on the screen and how human provides corrective demonstrations in an episode.
2. The second section is the footage of the MetaDrive human experiment, where the human expert interacts with the driving agent via a gamepad.
3. The third section shows the evaluation results of the PPL agent in a held-out MetaDrive test environment. We compare our approach PPL with the PVP baseline [28], and both agents are trained to 10K timesteps. The evaluation results show that our approach PPL has a higher test success rate and lower safety cost.
4. The fourth section shows the applicability of our methods to manipulation tasks in Robosuite [49]: Table Wiping and Nut Assembly. PPL successfully imitates the expert and accomplishes both tasks in evaluation environments.
5. In the fifth section, we provide a full training session on MetaDrive. The video is played at 5x speed, and it shows how a human expert trains a PPL agent on MetaDrive in under 12 minutes, with approximately 1.8K demonstration steps and 10K environment steps.

D Human Subject Research Protocol

Human Participants. Five university students (ages 20–30) with valid driver’s licenses and video gaming experience took part in the study voluntarily. After receiving a detailed overview of the procedures and providing written informed consent under an IRB-approved protocol, each participant completed a hands-on familiarization session. During this session, they were informed how the predicted trajectories were shown on screen, and they practiced with our control interface and learning environments until performing ten consecutive successful runs before the main experiments.

Main Experiment. Each participant began with one or two fully manual episodes to build confidence, and then ceded control to the agent when they felt safe. Participants were instructed to intervene only when the agent’s predicted trajectory appeared unsafe, illegal, or inconsistent with their desired actions. They were directed to prioritize safe task completion and then to guide the agent toward their personal driving or manipulation preferences.

E Notations

Before we prove Theorem 4.1, we recall all the notations in this work. We denote the human policy as π_h and the novice policy as π_n . For any stochastic policy $\pi(a | s)$ and the initial state distribution d_0 on state space \mathcal{S} , we define the value function $J(\pi)$ as the expected cumulative return: $J(\pi) = \mathbb{E}_{\tau \sim P_\pi} [\sum_{t=0}^{\infty} \gamma^t r(s_t, a_t)]$, wherein $\tau = (s_0, a_0, s_1, a_1, \dots)$ is the trajectory sampled from trajectory distribution P_π induced by π , d_0 and the state transition distribution \mathcal{P} . We also denote the Q-function of policy π as $Q(s, a) = \mathbb{E}_{\tau \sim P_\pi} [\sum_{t=0}^{\infty} \gamma^t r(s_t, a_t) | s_0 = s, a_0 = a]$. And we define the discounted state distribution under π as $d_\pi(s) = (1 - \gamma) \mathbb{E}_{\tau \sim P_\pi} [\sum_{t=0}^{\infty} \gamma^t \mathbb{I}[s_t = s]]$.

In our algorithm PPL, we have a preference dataset $\mathcal{D}_{\text{pref}}$ containing preference pairs (s, a^+, a^-) . The preference loss function of policy π in PPL is defined as

$$\mathcal{L}_{\text{pref}}(\pi) = |\mathcal{D}_{\text{pref}}|^{-1} \sum_{(s', a^+, a^-) \in \mathcal{D}_{\text{pref}}} [-\log \sigma(\beta \log \pi(a^+ | s) - \beta \log \pi(a^- | s))], \quad (7)$$

where β is a positive constant and $\sigma(x) = (1 + \exp(-x))^{-1}$ is the Sigmoid function.

We denote the state distribution in $\mathcal{D}_{\text{pref}}$ as

$$d_{\text{pref}}(s) = |\mathcal{D}_{\text{pref}}|^{-1} \sum_{(s', a^+, a^-) \in \mathcal{D}_{\text{pref}}} \mathbb{I}[s' = s]. \quad (8)$$

In addition, for any state s in $\mathcal{D}_{\text{pref}}$ with $d_{\text{pref}}(s) > 0$, we denote the empirical preference-pair distribution in state s as

$$\rho_{\text{pref}}^s(a_h, a_n) = \frac{\sum_{(s', a^+, a^-) \in \mathcal{D}_{\text{pref}}} \mathbb{I}[s' = s, a^+ = a_h, a^- = a_n]}{\sum_{(s', a^+, a^-) \in \mathcal{D}_{\text{pref}}} \mathbb{I}[s' = s]}, \quad (9)$$

which is a distribution on $\mathcal{A} \times \mathcal{A}$.

F Proof of Theorem 4.1

Our goal is to prove that the performance gap $J(\pi_h) - J(\pi_n)$ between the human policy π_h and the agent policy π_n can be bounded by the following three error terms: the state distribution shift δ_{dist} , the quality of preference labels δ_{pref} , and the optimization error ϵ . We denote the total variation for any two distributions P, Q on the same space as $D_{\text{TV}}(P, Q) = \frac{1}{2}\|P - Q\|_1$.

Here, we formally define the three error terms. The first state distribution shift error arises from the difference between the distribution of states in the preference dataset $\mathcal{D}_{\text{pref}}$ (denoted as $d_{\text{pref}}(s)$) and the discounted state distribution of the agent's policy π_n (denoted as $d_{\pi_n}(s)$). To define the distribution shift error δ_{dist} in PPL, we use the total variation between the two distributions, i.e.,

$$\delta_{\text{dist}} = D_{\text{TV}}(d_{\pi_n}, d_{\text{pref}}). \quad (10)$$

The second error term arises from the misalignment of the positive actions in the preference dataset, as the human action a_h in each tuple $(\tilde{s}_i, a_h, a_n) \in \mathcal{D}_{\text{pref}}$ is sampled in state s instead of the predicted future state \tilde{s}_i . In an ideal preference dataset, one would observe expert and novice actions drawn directly at \tilde{s}_i . To quantify this error, we define the following distribution $\rho_{\text{ideal}}^s(a_h, a_n) = \pi_h(a_h | s)\pi_n(a_n | s)$ on $\mathcal{A} \times \mathcal{A}$ for any state s , i.e., the distribution over pairs (a_h, a_n) if both policies were sampled at directly at state s . Then we use

$$\delta_{\text{pref}} = \mathbb{E}_{s \sim d_{\text{pref}}} D_{\text{TV}}(\rho_{\text{ideal}}^s, \rho_{\text{pref}}^s) \quad (11)$$

to define the errors in the preference dataset.

Finally, we define the optimization error of the agent policy π_n as

$$\epsilon = \mathcal{L}_{\text{pref}}(\pi_n) - \mathcal{L}_{\text{pref}}(\pi_h). \quad (12)$$

Under these notations, we have the following Thm. F.1. We note that when we choose a small $\beta \leq M^{-2}$ (M is defined in Thm. F.1), we have

$$J(\pi_h) - J(\pi_n) = \frac{1}{1-\gamma} \cdot O\left(\sqrt{\frac{\epsilon + 4 \log 2 \cdot \delta_{\text{pref}}}{2\beta}} + 2\delta_{\text{dist}}\right). \quad (13)$$

Theorem F.1 (Formal Statement of Theorem 4.1). *We denote the Q -function of the human policy π_h as $Q^*(s, a)$. We assume that for any (s, a, a') , $|Q^*(s, a) - Q^*(s, a')| \leq U$, $|\log \pi_h(a | s) - \log \pi_h(a' | s)| \leq M$, and $|\log \pi_n(a | s) - \log \pi_n(a' | s)| \leq M$, where U, M are positive constants. Then, we have*

$$J(\pi_h) - J(\pi_n) \leq \frac{U}{1-\gamma} \cdot \left(\sqrt{\frac{\epsilon + 4(\beta M + \log 2) \cdot \delta_{\text{pref}}}{2\beta}} + \frac{\beta M^2}{8} + 2\delta_{\text{dist}}\right). \quad (14)$$

Proof. The key is to combine Lem. F.2, Lem. F.3, and Lem. F.4 to obtain the bound.

From Lem. F.2, we can use the state distribution shift and the total variation of the two policies π_h, π_n on d_{pref} to bound the optimality gap:

$$J(\pi_h) - J(\pi_n) \leq \frac{U}{1-\gamma} \cdot \left(\mathbb{E}_{s \sim d_{\text{pref}}} D_{\text{TV}}(\pi_h(\cdot|s), \pi_n(\cdot|s)) + 2\delta_{\text{dist}} \right). \quad (15)$$

In addition, for any policy π , we define the function

$$g(\pi) = \mathbb{E}_{s \sim d_{\text{pref}}} \mathbb{E}_{a^+ \sim \pi_h(s), a^- \sim \pi_n(s)} [-\log \sigma(\beta \log \pi(a^+ | s) - \beta \log \pi(a^- | s))], \quad (16)$$

which represents the preference loss on ideal preference pairs, where a^+, a^- are sampled directly at each state s .

Using F.4, we can bound the total variation term $\mathbb{E}_{s \sim d_{\text{pref}}} D_{\text{TV}}(\pi_h(\cdot|s))$ by $g(\pi_n) - g(\pi_h)$:

$$\mathbb{E}_{s \sim d_{\text{pref}}} D_{\text{TV}}(\pi_h(\cdot|s), \pi_n(\cdot|s)) \leq \sqrt{\frac{g(\pi_n) - g(\pi_h)}{2\beta} + \frac{\beta M^2}{8}}. \quad (17)$$

In addition, by Lem. F.3, we can also bound $g(\pi_n) - g(\pi_h)$ by the optimization error ϵ on $\mathcal{L}_{\text{pref}}$ and the misalignment of preference levels δ_{pref} :

$$g(\pi_n) - g(\pi_h) \leq \epsilon + 4(\beta M + \log 2) \cdot \delta_{\text{pref}}. \quad (18)$$

Combining Eq. 15, 17, and 18 yields Eq. 14. \square

Lemma F.2 (Performance Optimality Gap on the State Distribution Shift). *We recall that $d_{\text{pref}}(s) = |\mathcal{D}_{\text{pref}}|^{-1} \mathbb{E}_{(s', a^+, a^-) \sim \mathcal{D}_{\text{pref}}} \mathbb{I}[s' = s]$, and we define $U = \max_{s \in \mathcal{S}, a_1, a_2 \in \mathcal{A}} |Q^*(s, a_1) - Q^*(s, a_2)|$.*

Then, for any two stochastic policies π_h, π_n , we have

$$J(\pi_h) - J(\pi_n) \leq \frac{U}{1-\gamma} \cdot \left(\mathbb{E}_{s \sim d_{\text{pref}}} D_{\text{TV}}(\pi_h(\cdot|s), \pi_n(\cdot|s)) + 2\delta_{\text{dist}} \right). \quad (19)$$

where $\delta_{\text{dist}} = D_{\text{TV}}(d_{\pi_n}, d_{\text{pref}})$.

Proof Sketch. The key is to use the Performance Difference Lemma (Lem. G.2) on $J(\pi_h) - J(\pi_n)$, yielding Eq. 20. Then, we can apply Lem. G.1, which bounds the expectation on $s \sim d_{\text{pref}}$ and $s \sim d_{\pi_n}$ by the distribution shift term δ_{dist} . Finally, applying the assumption $U = \max_{s \in \mathcal{S}, a_1, a_2 \in \mathcal{A}} |Q^*(s, a_1) - Q^*(s, a_2)|$ bounds the difference of the Q-function by the total variation between π_h and π_n . \square

Proof. By the Performance Difference Lemma (Lem. G.2), we have

$$J(\pi_h) - J(\pi_n) = \frac{1}{1-\gamma} \mathbb{E}_{s \sim d_{\pi_n}} \mathbb{E}_{a_h \sim \pi_h(s), a_n \sim \pi_n(s)} [Q^*(s, a_h) - Q^*(s, a_n)]. \quad (20)$$

By Lem. G.1, as d_{π_n} and d_{pref} are two distributions on the same state space \mathcal{S} , we have

$$\begin{aligned} & (1-\gamma)(J(\pi_h) - J(\pi_n)) \\ & \leq \mathbb{E}_{s \sim d_{\text{pref}}} \mathbb{E}_{a_h \sim \pi_h(s), a_n \sim \pi_n(s)} [Q^*(s, a_h) - Q^*(s, a_n)] \\ & \quad + 2D_{\text{TV}}(d_{\pi_n}, d_{\text{pref}}) \cdot \max_{s \in \mathcal{S}} \left| \mathbb{E}_{a_h \sim \pi_h(s), a_n \sim \pi_n(s)} [Q^*(s, a_h) - Q^*(s, a_n)] \right| \\ & \leq \mathbb{E}_{s \sim d_{\text{pref}}} \mathbb{E}_{a_h \sim \pi_h(s), a_n \sim \pi_n(s)} [Q^*(s, a_h) - Q^*(s, a_n)] \\ & \quad + 2\delta_{\text{dist}} \cdot \max_{s \in \mathcal{S}} \mathbb{E}_{a_h \sim \pi_h(s), a_n \sim \pi_n(s)} |Q^*(s, a_h) - Q^*(s, a_n)| \\ & \leq \mathbb{E}_{s \sim d_{\text{pref}}} \left[\mathbb{E}_{a_h \sim \pi_h(s)} Q^*(s, a_h) - \mathbb{E}_{a_n \sim \pi_n(s)} Q^*(s, a_n) \right] + 2U \cdot \delta_{\text{dist}}, \end{aligned} \quad (21)$$

where we use $U = \max_{s \in \mathcal{S}, a_1, a_2 \in \mathcal{A}} |Q^*(s, a_1) - Q^*(s, a_2)|$ in the last inequality of Eq. 21.

In addition, $\pi_h(s)$ and $\pi_n(s)$ are two probability distributions on the same action space \mathcal{A} . By Lem. G.1, we have for any $s \in \mathcal{S}$,

$$\mathbb{E}_{a_h \sim \pi_h(s)} Q^*(s, a_h) - \mathbb{E}_{a_n \sim \pi_n(s)} Q^*(s, a_n) \leq U \cdot D_{\text{TV}}(\pi_h(\cdot|s), \pi_n(\cdot|s)). \quad (22)$$

This proves that

$$J(\pi_h) - J(\pi_n) \leq \frac{U}{1-\gamma} \cdot \left(\mathbb{E}_{s \sim d_{\text{pref}}} D_{\text{TV}}(\pi_h(\cdot|s), \pi_n(\cdot|s)) + 2\delta_{\text{dist}} \right). \quad (23)$$

□

Lemma F.3 (Misalignment of Preference Pairs). *We recall that the loss function of the policy π is $\mathcal{L}_{\text{pref}}(\pi) = -\mathbb{E}_{(s, a^+, a^-) \sim \mathcal{D}_{\text{pref}}} [\log \sigma(\beta \log \pi(a^+|s) - \beta \log \pi(a^-|s))]$. And the optimization loss is defined as $\epsilon = \mathcal{L}_{\text{pref}}(\pi_n) - \mathcal{L}_{\text{pref}}(\pi_h)$.*

In addition, following Eq. 16, for any policy π , we define

$$g(\pi) = \mathbb{E}_{s \sim d_{\text{pref}}} \mathbb{E}_{a^+ \sim \pi_h(s), a^- \sim \pi_n(s)} [-\log \sigma(\beta \log \pi(a^+|s) - \beta \log \pi(a^-|s))]. \quad (24)$$

Under the assumption that for any (s, a, a') , $|\log \pi_h(a|s) - \log \pi_h(a'|s)| \leq M$, and $|\log \pi_n(a|s) - \log \pi_n(a'|s)| \leq M$, we have

we can bound

$$g(\pi_n) - g(\pi_h) \leq \epsilon + 4(\beta M + \log 2) \cdot \delta_{\text{pref}}, \quad (25)$$

where $\delta_{\text{pref}} = \mathbb{E}_{s \sim d_{\text{pref}}} D_{\text{TV}}(\rho_{\text{ideal}}^s, \rho_{\text{pref}}^s)$.

Proof Sketch. The key is to apply Lem. G.1 on the two distributions ρ_{ideal}^s and ρ_{pref}^s , so that we can bound the difference of $\mathcal{L}_{\text{pref}}(\pi)$ and $g(\pi)$ for any policy π by $O(\delta_{\text{pref}})$. □

Proof. For any $s \in \mathcal{S}$, we denote $\rho_{\text{ideal}}^s(a_h, a_n) = \pi_h(a_h|s)\pi_n(a_n|s)$, a probability distribution on $\mathcal{A} \times \mathcal{A}$. We also denote $\rho_{\text{pref}}^s(a_h, a_n) = \rho_{\text{pref}}(s, a_h, a_n)/d_{\text{pref}}(s)$ for any s such that $d_{\text{pref}}(s) > 0$, where we recall that $\rho_{\text{pref}}(s, a_h, a_n) = |\mathcal{D}_{\text{pref}}|^{-1} \mathbb{E}_{(s', a^+, a^-) \sim \mathcal{D}_{\text{pref}}} \mathbb{I}[s' = s, a^+ = a_h, a^- = a_n]$.

The key is that ρ_{ideal}^s and ρ_{pref}^s are two distributions on the same space $\mathcal{A} \times \mathcal{A}$, and we can apply Lem. G.1 on Eq. 24 to obtain the proof.

We denote $l^\pi(s, a^+, a^-) = -\log \sigma(\beta \log \pi(a^+|s) - \beta \log \pi(a^-|s))$.

We also denote $l_{\text{max}}^\pi = \max_{s, a^+, a^-} |l^\pi(s, a^+, a^-)|$, and $l_{\text{max}} = \max(l_{\text{max}}^{\pi_h}, l_{\text{max}}^{\pi_n})$. Then, for any policy π ,

$$\begin{aligned} g(\pi) &= \mathbb{E}_{s \sim d_{\text{pref}}} \mathbb{E}_{a^+ \sim \pi_h(s), a^- \sim \pi_n(s)} l^\pi(s, a^+, a^-) \\ &= \mathbb{E}_{s \sim d_{\text{pref}}} \mathbb{E}_{(a^+, a^-) \sim \rho_{\text{ideal}}^s} l^\pi(s, a^+, a^-) \\ &\leq \mathbb{E}_{s \sim d_{\text{pref}}} \left[2l_{\text{max}}^\pi \cdot D_{\text{TV}}(\rho_{\text{ideal}}^s, \rho_{\text{pref}}^s) + \mathbb{E}_{(a^+, a^-) \sim \rho_{\text{pref}}^s} l^\pi(s, a^+, a^-) \right] \\ &= 2l_{\text{max}}^\pi \delta_{\text{pref}} + \mathbb{E}_{s \sim d_{\text{pref}}} \mathbb{E}_{(a^+, a^-) \sim \rho_{\text{pref}}^s} l^\pi(s, a^+, a^-) \\ &= 2l_{\text{max}}^\pi \delta_{\text{pref}} + |\mathcal{D}_{\text{pref}}|^{-1} \sum_{(s, a^+, a^-) \in \mathcal{D}_{\text{pref}}} l^\pi(s, a^+, a^-) \\ &= 2l_{\text{max}}^\pi \delta_{\text{pref}} + \mathcal{L}_{\text{pref}}(\pi). \end{aligned} \quad (26)$$

Similarly, we can obtain that $g(\pi) \geq -2l_{\text{max}}^\pi \delta_{\text{pref}} + \mathcal{L}_{\text{pref}}(\pi)$ for any policy π . Thus we have

$$g(\pi_n) - g(\pi_h) \leq 4l_{\text{max}} \delta_{\text{pref}} + (\mathcal{L}_{\text{pref}}(\pi_n) - \mathcal{L}_{\text{pref}}(\pi_h)) = 4l_{\text{max}} \delta_{\text{pref}} + \epsilon. \quad (27)$$

Finally, under the condition that $|\log \pi(a|s) - \log \pi(a'|s)| \leq M$ for any (s, a, a') , we have $|l^\pi(s, a, a')| \leq -\log \sigma(-\beta M) = \log(1 + \exp(\beta M)) \leq \beta M + \log 2$.

This implies that $l_{\max} \leq \beta M + \log 2$ and completes the proof. \square

Lemma E.4 (Optimization Error Bounds the Total Variation). *We assume that for any (s, a, a') , $|\log \pi_h(a|s) - \log \pi_h(a'|s)| \leq M$, and $|\log \pi_n(a|s) - \log \pi_n(a'|s)| \leq M$.*

We recall that $g(\pi) = \mathbb{E}_{s \sim d_{\text{pref}}} \mathbb{E}_{a^+ \sim \pi_h(s), a^- \sim \pi_n(s)} [-\log \sigma(\beta \log \pi(a^+|s) - \beta \log \pi(a^-|s))]$, which is defined in Eq. 16. Then we have

$$\mathbb{E}_{s \sim d_{\text{pref}}} D_{\text{TV}}(\pi_h(\cdot|s), \pi_n(\cdot|s)) \leq \sqrt{\frac{g(\pi_n) - g(\pi_h)}{2\beta} + \frac{\beta M^2}{8}}. \quad (28)$$

Proof Sketch. First, we define

$$f(\pi) = -\frac{\beta}{2} \mathbb{E}_{s \sim d_{\text{pref}}} \mathbb{E}_{a^+ \sim \pi_h(s), a^- \sim \pi_n(s)} [\log \pi(a^+|s) - \log \pi(a^-|s)] + \log 2. \quad (29)$$

Using the Taylor's expansion on the function $\log \sigma(x)$ at $x = 0$, when the policy π satisfies $|\log \pi(a|s) - \log \pi(a'|s)| \leq M$ for any (s, a, a') , we can obtain that $|g(\pi) - f(\pi)| \leq \frac{\beta^2 M^2}{8}$.

In addition, $f(\pi_n) - f(\pi_h)$ bounds the KL divergence of the two policies π_h and π_n over $s \sim d_{\text{pref}}$. So we can use Pinsker's inequality to obtain the bound on $D_{\text{TV}}(\pi_h(\cdot|s), \pi_n(\cdot|s))$. \square

Proof. For any (s, a^+, a^-) , we denote $u_n(s, a^+, a^-) = \log \pi_n(a^+|s) - \log \pi_n(a^-|s)$, and $u_h(s, a^+, a^-) = \log \pi_h(a^+|s) - \log \pi_h(a^-|s)$. From the assumptions, we can obtain that $|u_n(s, a^+, a^-)| \leq M$ and $|u_h(s, a^+, a^-)| \leq M$.

By definition of the function $g(\cdot)$, we have $g(\pi_n) - g(\pi_h) = \mathbb{E}_{s \sim d_{\text{pref}}} \mathbb{E}_{a^+ \sim \pi_h(s), a^- \sim \pi_n(s)} [\log \sigma(\beta \cdot u_h(s, a^+, a^-)) - \log \sigma(\beta \cdot u_n(s, a^+, a^-))]$.

The Taylor's expansion of $\log \sigma(x)$ at $x = 0$ ensures that for any $x \in \mathbb{R}$, we have

$$\left| \log \sigma(x) + \log 2 - \frac{1}{2}x \right| \leq \frac{1}{8}x^2. \quad (30)$$

This ensures that

$$\begin{aligned} g(\pi_n) &= \mathbb{E}_{s \sim d_{\text{pref}}} \mathbb{E}_{a^+ \sim \pi_h(s), a^- \sim \pi_n(s)} [-\log \sigma(\beta \cdot u_n(s, a^+, a^-))] \\ &\geq \log 2 - \frac{\beta}{2} \mathbb{E}_{s \sim d_{\text{pref}}} \mathbb{E}_{a^+ \sim \pi_h(s), a^- \sim \pi_n(s)} u_n(s, a^+, a^-) - \frac{\beta^2 M^2}{8}, \end{aligned} \quad (31)$$

and similarly,

$$\begin{aligned} g(\pi_h) &= \mathbb{E}_{s \sim d_{\text{pref}}} \mathbb{E}_{a^+ \sim \pi_h(s), a^- \sim \pi_n(s)} [-\log \sigma(\beta \cdot u_h(s, a^+, a^-))] \\ &\leq \log 2 - \frac{\beta}{2} \mathbb{E}_{s \sim d_{\text{pref}}} \mathbb{E}_{a^+ \sim \pi_h(s), a^- \sim \pi_n(s)} u_h(s, a^+, a^-) + \frac{\beta^2 M^2}{8}, \end{aligned} \quad (32)$$

Hence, we have

$$\begin{aligned} g(\pi_n) - g(\pi_h) &\geq \frac{\beta}{2} \mathbb{E}_{s \sim d_{\text{pref}}} \mathbb{E}_{a^+ \sim \pi_h(s), a^- \sim \pi_n(s)} [u_h(s, a^+, a^-) - u_n(s, a^+, a^-)] - \frac{\beta^2 M^2}{4} \\ &= \frac{\beta}{2} \mathbb{E}_{s \sim d_{\text{pref}}} \mathbb{E}_{a^+ \sim \pi_h(s), a^- \sim \pi_n(s)} \left[\log \frac{\pi_h(a^+|s)}{\pi_h(a^-|s)} - \log \frac{\pi_n(a^+|s)}{\pi_n(a^-|s)} \right] - \frac{\beta^2 M^2}{4} \\ &= \frac{\beta}{2} \mathbb{E}_{s \sim d_{\text{pref}}} \left[\mathbb{E}_{a^+ \sim \pi_h(s)} \log \frac{\pi_h(a^+|s)}{\pi_n(a^+|s)} + \mathbb{E}_{a^- \sim \pi_n(s)} \log \frac{\pi_n(a^-|s)}{\pi_h(a^-|s)} \right] - \frac{\beta^2 M^2}{4}. \end{aligned} \quad (33)$$

By the definition of KL divergence, we have

$$\begin{aligned} g(\pi_n) - g(\pi_h) &= \frac{\beta}{2} \mathbb{E}_{s \sim d_{\text{pref}}} \left[\text{KL}\left(\pi_h(\cdot|s) \middle\| \pi_n(\cdot|s)\right) + \text{KL}\left(\pi_n(\cdot|s) \middle\| \pi_h(\cdot|s)\right) \right] - \frac{\beta^2 M^2}{4} \\ &\geq 2\beta \mathbb{E}_{s \sim d_{\text{pref}}} \left[D_{\text{TV}}(\pi_h(\cdot|s), \pi_n(\cdot|s)) \right]^2 - \frac{\beta^2 M^2}{4}, \end{aligned} \quad (34)$$

where we use Pinsker's inequality to obtain the bound on $D_{\text{TV}}(\pi_h(\cdot|s), \pi_n(\cdot|s))$ from the KL divergence.

Finally, we apply the inequality $\mathbb{E}[X^2] \geq (\mathbb{E}[X])^2$ on $X = D_{\text{TV}}(\pi_h(\cdot|s), \pi_n(\cdot|s))$, so that we have

$$g(\pi_n) - g(\pi_h) \geq 2\beta \left[\mathbb{E}_{s \sim d_{\text{pref}}} D_{\text{TV}}(\pi_h(\cdot|s), \pi_n(\cdot|s)) \right]^2 - \frac{\beta^2 M^2}{4}. \quad (35)$$

This proves that

$$\mathbb{E}_{s \sim d_{\text{pref}}} D_{\text{TV}}(\pi_h(\cdot|s), \pi_n(\cdot|s)) \leq \sqrt{\frac{g(\pi_n) - g(\pi_h)}{2\beta} + \frac{\beta M^2}{8}}. \quad (36)$$

□

G Technical Lemmas

Lemma G.1 (Expectation Difference via Total Variation). *Let P and Q be two probability distributions on a measurable space \mathcal{X} , and let $f: \mathcal{X} \rightarrow \mathbb{R}$ be any measurable function satisfying the uniform bound $|f(x)| \leq M$ for any $x \in \mathcal{X}$. Then*

$$\left| \mathbb{E}_{x \sim P(\cdot)} f(x) - \mathbb{E}_{x \sim Q(\cdot)} f(x) \right| \leq 2M \cdot D_{\text{TV}}(P, Q), \quad (37)$$

where $D_{\text{TV}}(P, Q) = \frac{1}{2} \|P - Q\|_1$ is the total variation distance.

In addition, when the measurable function g satisfies the bound $|g(x_1) - g(x_2)| \leq M'$ for any $x_1, x_2 \in \mathcal{X}$, we have

$$\left| \mathbb{E}_{x \sim P(\cdot)} g(x) - \mathbb{E}_{x \sim Q(\cdot)} g(x) \right| \leq M' \cdot D_{\text{TV}}(P, Q). \quad (38)$$

Proof. When $|f(x)| \leq M$ for any x , we have

$$\begin{aligned} \left| \mathbb{E}_{x \sim P(\cdot)} f(x) - \mathbb{E}_{x \sim Q(\cdot)} f(x) \right| &= \left| \sum_x f(x) \cdot (P(x) - Q(x)) \right| \\ &\leq \sum_x |f(x)| \cdot |P(x) - Q(x)| \\ &\leq M \cdot \sum_x |P(x) - Q(x)| \\ &= 2M \cdot D_{\text{TV}}(P, Q). \end{aligned} \quad (39)$$

When $|g(x_1) - g(x_2)| \leq M'$ for any $x_1, x_2 \in \mathcal{X}$, we set $f(x) = g(x) - \frac{1}{2}c$, where $c = \sup_{x \in \mathcal{X}} f(x) + \inf_{x \in \mathcal{X}} f(x)$. As we have $|f(x)| \leq M'/2$ for any $x \in \mathcal{X}$, we have

$$\left| \mathbb{E}_{x \sim P(\cdot)} g(x) - \mathbb{E}_{x \sim Q(\cdot)} g(x) \right| = \left| \mathbb{E}_{x \sim P(\cdot)} f(x) - \mathbb{E}_{x \sim Q(\cdot)} f(x) \right| \leq M' \cdot D_{\text{TV}}(P, Q). \quad (40)$$

□

Lemma G.2 (Performance Gap Between Human Policy and Novice Policy). *We denote the Q-function of human policy π_h as $Q^*(s, a) = \mathbb{E}_{\tau \sim P_{\pi_h}} [\sum_{t=0}^{\infty} \gamma^t r(s_t, a_t) | s_0 = s, a_0 = a]$.*

For the human policy π_h and the novice policy π_n whose value functions are $J(\pi_h), J(\pi_n)$, respectively, we have

$$J(\pi_h) - J(\pi_n) = \frac{1}{1-\gamma} \mathbb{E}_{s \sim d_{\pi_n}} \left[\mathbb{E}_{a_h \sim \pi_h(s)} Q^*(s, a_h) - \mathbb{E}_{a_n \sim \pi_n(s)} Q^*(s, a_n) \right]. \quad (41)$$

Proof. We denote the Q-function of novice policy π_n as $Q_n(s, a) = \mathbb{E}_{\tau \sim P_{\pi_n}} [\sum_{t=0}^{\infty} \gamma^t r(s_t, a_t) | s_0 = s, a_0 = a]$.

We denote value functions of π_h, π_n as $V^*(s) = \mathbb{E}_{a \sim \pi_h(s)} Q^*(s, a)$ and $V_n(s) = \mathbb{E}_{a \sim \pi_n(s)} Q_n(s, a)$, respectively. And we have $J(\pi_h) = \mathbb{E}_{s_0 \sim d_0} V^*(s_0)$, and $J(\pi_n) = \mathbb{E}_{s_0 \sim d_0} V_n(s_0)$.

We define the advantage function of π_h as $A^*(s, a) = Q^*(s, a) - V^*(s)$.

By the performance difference lemma (Lemma 6.1, [14]), we have

$$\mathbb{E}_{s_0 \sim d_0} [V_n(s_0) - V^*(s_0)] = \frac{1}{1-\gamma} \mathbb{E}_{s \sim d_{\pi_n}} \left[\mathbb{E}_{a \sim \pi_n(s)} A^*(s, a) \right]. \quad (42)$$

This implies that

$$\begin{aligned} \mathbb{E}_{s_0 \sim d_0} [V_n(s_0) - V^*(s_0)] &= \frac{1}{1-\gamma} \mathbb{E}_{s \sim d_{\pi_n}} \left[\mathbb{E}_{a \sim \pi_n(s)} [Q^*(s, a) - V^*(s)] \right] \\ &= \frac{1}{1-\gamma} \mathbb{E}_{s \sim d_{\pi_n}} \left[-V^*(s) + \mathbb{E}_{a \sim \pi_n(s)} Q^*(s, a) \right] \\ &= \frac{1}{1-\gamma} \mathbb{E}_{s \sim d_{\pi_n}} \left[-\mathbb{E}_{a \sim \pi_h(s)} Q^*(s, a) + \mathbb{E}_{a \sim \pi_n(s)} Q^*(s, a) \right]. \end{aligned} \quad (43)$$

Multiplying -1 on both sides, we can obtain that

$$J(\pi_h) - J(\pi_n) = \frac{1}{1-\gamma} \mathbb{E}_{s \sim d_{\pi_n}} \left[\mathbb{E}_{a_h \sim \pi_h(s)} Q^*(s, a_h) - \mathbb{E}_{a_n \sim \pi_n(s)} Q^*(s, a_n) \right]. \quad (44)$$

□

H Ethics Statement

Our Predictive Preference Learning from Human Interventions (PPL) delivers a human-friendly, human-in-the-loop training process that increases automation while minimizing expert effort, advancing more intelligent AI systems with reduced human burden. All the experiments are conducted entirely in simulation, ensuring no physical risk to participants. All volunteers provided informed consent, were compensated above local market rates, and could pause or withdraw from the study at any time without penalty. Individual sessions lasted less than one hour, with a mandatory rest period of at least three hours before any subsequent participation. No personal or sensitive data was collected or shared. We have obtained the IRB approval to conduct this project.

While PPL promises positive social impact by streamlining human-AI collaboration, it may also encourage overreliance on automated systems or inherit biases present in expert involvement.